Title
Methodology for Validation of Simulated Ground Motions for Seismic Response Assessment: Application to CyberShake Source-Based Ground Motions

Journal
Bulletin of the Seismological Society of America, 111(1)

ISSN
0037-1106

Authors
Fayaz, Jawad
Azar, Sarah
Dabaghi, Mayssa
et al.

Publication Date
2021-02-01

DOI
10.1785/0120200240

Peer reviewed

Methodology for Validation of Simulated Ground Motions for Seismic Response Assessment: Application to CyberShake Source-Based Ground Motions

Jawad Fayaz[1], Sarah Azar[2], Mayssa Dabaghi[2], and Farzin Zareian[*1]

ABSTRACT

A comprehensive methodology for the validation of simulated ground motions is presented. The suggested methodology can be geared toward any ground-motion simulation method and seismic response assessment, in a target engineering application. The methodology is founded on the comparison between conforming groups of ground-motion waveforms from recordings and simulations and their effect on a representative collection of structures that represent the engineering application. The comparison considers the statistics of earthquake scenarios at the level of the event and site parameters, the resulting waveform characteristics, and the subsequent structural responses. Regression models are developed at three levels (between structural responses and waveform characteristics, structural responses and event and site parameters, and waveform characteristics and event and site parameters). Similarities between the models from groups of recorded and simulated ground motions guide the validation process. The validation methodology is applied to CyberShake (v.15.12) simulations and for the estimation of the column drift ratio of a bridge structure. It is shown that CyberShake (v.15.12) can be used to assess the median seismic response of the used bridge. Some discrepancies between simulations and recordings are observed, which could be attributed to the basin and site-response models used for simulations. Further implementation and refinement of the suggested methodology are recommended to make broader conclusions.

KEY POINTS

- A comprehensive methodology for the validation of simulated ground motions is presented.
- Its application is demonstrated for CyberShake (v.15.12) simulated motions and a Standard Ordinary Bridge.
- The methodology can be implemented for any ground-motion simulation method and target engineering application.

INTRODUCTION

The mainstream approach for the design of structures to withstand impacts of seismic hazard is to utilize a set of selected and modified ground motions from past recorded worldwide events. Such an approach does not provide the opportunity to embrace the advancements in ground-motion simulation, which can result in waveforms tailored for the structures' location. The main hurdle in using simulated motions is the lack of consensus on the acceptable accuracy in the estimated structural responses they result in (Jones and Zareian, 2010; Bradley *et al.*, 2017; Bayless and Abrahamson, 2018).

Researchers have responded to the professional and intellectual need for developing validation methods for simulated ground motions. These efforts can be categorized into three main types of validation approaches. Type I validation methods are based on historic events (Galasso *et al.*, 2012, 2013, 2018; Goulet *et al.*, 2015; Rezaeian *et al.*, 2015; Tsioulou *et al.*, 2019). They show if ground-motion waveforms obtained from replicating a single event at their respective recording stations have the same central value of response (i.e., of Multi-Degree-of-Freedom or Single-Degree-of-Freedom systems) as their

1. Department of Civil & Environmental Engineering, University of California, Irvine, Irvine, California, U.S.A.; 2. Department of Civil & Environmental Engineering, American University of Beirut, Beirut, Lebanon

*Corresponding author: zareian@uci.edu

Cite this article as Fayaz, J., S. Azar, M. Dabaghi, and F. Zareian (2020). Methodology for Validation of Simulated Ground Motions for Seismic Response Assessment: Application to CyberShake Source-Based Ground Motions, *Bull. Seismol. Soc. Am.* **111**, 226–241, doi: 10.1785/0120200240

corresponding recordings. Type II validation methods focus on the similarity of trends in important parameters that represent ground-motion characteristics (e.g., peak ground acceleration [PGA], building response) with event and site parameters obtained from simulations and recordings (Star *et al.*, 2011). In contrast with type I validation, type II validation may utilize a population of past events to form the trends in ground-motion parameters. Type III validation methods (Zhong, 2016; Bijelić *et al.*, 2019) were suggested to find the equivalency between simulated and recorded ground motions using established structural and earthquake engineering principles and statistical tools; similarity of response spectra is the cornerstone of such equivalency checks. Type III validation is intended to encourage engineers to utilize simulated ground motions, similarly to recorded motions, in seismic design or risk assessment applications.

The validation methodology proposed in this article compares the seismic response of structures representative of an engineering application and the ground-motion waveform characteristics (or ground-motion parameters) for catalogs of simulated and recorded ground motions that contain a wide range of scenarios. These catalogs are collected in a way that ensures similar ranges, and, when possible, distributions of the earthquake event and site parameters in the different catalogs. In contrast to type I validation methods, the proposed methodology does not require the scenarios (i.e., the event and site parameters) to be identical in the different catalogs and does not directly compare the statistics of the ground-motion parameters or their subsequent structural responses. Instead, the trends or scaling of the structural responses (or engineering demand parameters [EDPs]) and ground-motion parameters with the event and site parameters (denoted by $\boldsymbol{\theta}$) are compared between the different catalogs, as well as the scaling of the structural responses with the ground-motion parameters. This is achieved by developing, for each catalog, regression models that relate $\boldsymbol{\theta} \rightarrow$ EDP, $\boldsymbol{\theta} \rightarrow \mathbf{RZZ_s}$, and $\mathbf{RZZ_s} \rightarrow$ EDP, in which $\mathbf{RZZ_s}$, as described in later sections, represents a suggested set of important parameters that characterize the ground-motion waveforms. The regression functional forms should account, to the extent possible, for the physics of earthquakes, wave propagation, and structural response. The proposed methodology gauges the validity of a ground-motion simulation procedure for a specific engineering application by evaluating the statistical similarity of the trends of EDP$|\boldsymbol{\theta}$, $\mathbf{RZZ_s}|\boldsymbol{\theta}$, and EDP$|\mathbf{RZZ_s}$ (in which $|$ is read as given) in the recorded and simulated catalogs, and, in particular, the regression coefficients, which describe the mean relation, and the root mean square error (rmse), which describes the variability. The methodology presented herein can, therefore, be categorized as a type II validation approach. The main contribution of the suggested validation methodology resides in its ability to be tailored for the target simulation method and engineering application, while founded on a set of established engineering principles and statistical tools. In this article, CyberShake simulations (v.15.12) (Graves *et al.*, 2011; hereafter referred to as CyberShake) and a bridge structure are utilized to showcase the validation methodology.

PROPOSED METHODOLOGY

The validation methodology presented in this article is described in the following steps.

Step 1: For the region of interest, obtain the set of recorded ground motions and develop $n(> 50)$ catalogs of statistically conforming simulated ground motions

The proposed methodology is founded on the comparison between two conforming groups of ground-motion waveforms and their effect on a representative collection of structures (representing the engineering application). The first group consists of n catalogs of waveforms obtained from the ground-motion simulation method being validated. The second group consists of a single catalog of waveforms from recordings of past seismic events. These two groups of ground motions should be obtained from a conforming collection of seismic events and recording stations, to ensure that the statistics of $\boldsymbol{\theta}$ are similar. The vector $\boldsymbol{\theta}$ includes parameters that describe the earthquake source, the path, and the characteristics of the sites, such as the earthquake moment magnitude (M_w), the closest distance to the coseismic fault rupture plane (R_{rup}), and the time-averaged shear-wave velocity in the top 30 m of the site (V_{S30}). Other parameters used in ground-motion models (GMMs), such as proposed by Campbell and Bozorgnia (2014, 2019), can also be employed and are presented in more detail in a later section. For a reliable comparison of simulated and recorded ground motions, the two types of datasets should also be consistent in terms of their size (number of events and records), time span, and geographic location. Hence, any differences observed at the level of ground-motion parameters or seismic response can be attributed to differences in the ground motions, and not to inconsistencies in the datasets.

Therefore, in the first step of the methodology, the usable ground motions recorded in the region of interest are collected from the available database, and the time span of the recorded seismicity of the region is represented as TS years. A collection of $n(> 50)$ earthquake catalogs of synthetic ground motions is then collected. The catalogs should represent TS years of seismicity in the region and should be statistically conforming (in their ranges, and when possible, distributions) to the recorded ground motions in terms of their vector $\boldsymbol{\theta}$. This can be done using an appropriate earthquake rupture forecast model (for the distribution of magnitudes) and site sampling methods (for conforming distances and site conditions) and tested using various statistical measures such as the Kullback–Leibler (KL) divergence, Kolmogorov–Smirnov test, and so forth.

Step 2: Conduct nonlinear time-history analysis (NLTHA) of the target structure to obtain the EDPs for the recorded catalog and the n catalogs of simulated ground motions

The primary goal of the methodology is to validate a simulation method for a target engineering application; therefore, understanding the impact of ground-motion parameters on the response of structures is necessary to validate the simulation method at the level of the EDPs. In this context, NLTHA of the target structure are conducted to calculate the seismic response and the EDPs for the recorded catalog and the n catalogs of simulated ground motions, using the rotated components of the ground motions in the different catalogs. To be consistent with the orientation of ground motions, the two horizontal components of all the recorded and simulated ground motions are rotated to the direction of largest Arias intensity, termed as *major*, and its orthogonal component, termed as *minor*, as per Rezaeian and Der Kiureghian (2010). The rotated ground motions are then applied to the target structure, and the required EDPs are computed.

Step 3: Compute the **RZZ** parameters of all the recorded and simulated ground motions, and select the important **RZZ** parameters that sufficiently describe the EDP of the target structure.

The waveform characteristics (denoted as **RZZ**) are first determined for all the recorded and simulated ground motions. **RZZ** is a vector of ground-motion parameters and is named after the initials of researchers Rezaeian, Zhong, and Zareian (Rezaeian *et al.*, 2015). The parameters in the vector are borrowed from Rezaeian and Der Kiureghian (2010) and Dabaghi and Der Kiureghian (2018), to describe the intensity, duration, and frequency content characteristics of the two horizontal components of a seismic excitation. The **RZZ** vector includes the Arias intensity (I_A), significant durations (D_{5-95}, D_{0-30}, D_{0-5}), and time to the middle of the strong shaking phase (t_{mid}) defined as the time to the 30% level of I_A for $R_{rup} \leq 30$ km (Dabaghi and Der Kiureghian, 2018), and 45% level of I_A for $R_{rup} > 30$ km (Rezaeian and Der Kiureghian, 2010). These parameters describe the time modulating function that accounts for the temporal nonstationarity of each ground-motion component. The vector also has components to represent the evolutionary frequency content of ground motions, including the filter frequency at t_{mid} (f_{mid}) and the rate of change of the filter frequency with time (f'). The bandwidth of the process is further defined by the filter damping ratio parameter (ξ). Hence, the eight parameters of the **RZZ** vector (I_A, D_{5-95}, D_{0-30}, D_{0-5}, t_{mid}, f_{mid}, f', ξ) are computed for the major and minor horizontal components of each ground motion. Therefore, each ground motion is associated with an **RZZ** vector of 16 parameters.

After determining the **RZZ** vector for each ground motion in the recorded and simulated catalogs, a feature selection is conducted to select the important **RZZ** parameters that sufficiently describe the EDP of the target structure. In other words, the selected parameters are a subset of the **RZZ** parameters that are statistically meaningful in predicting the EDP for the target structure. Feature selection algorithms (e.g., random forests, stepwise regressions) can be used to identify which **RZZ** parameters are important for the target EDP. The feature selection is conducted for the recorded catalog and each of the n simulated catalogs separately. Then the **RZZ** parameters that are deemed important by most of the n simulated catalogs and the one recorded set are obtained. The union of these two obtained important **RZZ** vectors forms the important **RZZ** parameters. It should be noted that the important **RZZ** vector is specific to the target structure and to the EDP considered in the application.

Step 4: Among the important **RZZ** parameters, drop the collinear parameters, and obtain the finalized subset of $\mathbf{RZZ_s}$ parameters that can describe the EDP of the target structure

To minimize the effects of collinearity among the important **RZZ** parameters, a collinearity check is conducted using measures such as the variance inflation factor (VIF) and correlation coefficients. This collinearity check is performed for the recorded catalog and each of the n simulated catalogs separately. Then the **RZZ** parameters that are deemed correlated by most of the n simulated catalogs and the one recorded catalog are removed sequentially until collinearity is reduced satisfactorily in all catalogs. In some cases, step 4 can be combined with step 3, in which some algorithms may be able to perform feature selection, while minimizing the selection of correlated parameters.

Step 5: Using the $\mathbf{RZZ_s}$ parameters, develop and compare regression equations, to estimate the EDP ($\mathbf{RZZ_s} \rightarrow$ EDP) between the recorded set and the n catalogs of simulated ground motions

The relation between $\mathbf{RZZ_s}$ and EDP characterizes the importance of $\mathbf{RZZ_s}$ parameters in obtaining EDP. For both the recorded catalog and n simulated catalogs, independent regressions are conducted using the $\mathbf{RZZ_s}$ parameters, to estimate the EDPs of the target structure. This leads to one set of coefficients for the recorded catalog and n sets of coefficients for the n simulated catalogs. These coefficients represent the effect of the $\mathbf{RZZ_s}$ parameters on the EDPs obtained using the recorded and the n simulated catalogs. The set of coefficients from the recorded catalog is statistically compared against the n sets of coefficients from the simulated catalogs, to validate whether the relationship between these $\mathbf{RZZ_s}$ and EDP is consistent in simulated and recorded motions.

Step 6: Using the event and site parameters and appropriate functional forms, develop and compare regression equations to estimate the EDPs ($\boldsymbol{\theta} \rightarrow$ EDP) between the recorded catalog and the n catalogs of simulated ground motions

For both the recorded catalog and the n simulated catalogs, independent regressions between the event and site parameters $\boldsymbol{\theta}$ and the EDPs of the target structure are conducted using an appropriate functional form. The fitted regression coefficients represent the effect of the physics of the rupture, wave propagation, and site effects on the EDPs obtained using the recorded and n simulated catalogs. The set of coefficients from the recorded catalog is statistically compared against the n sets

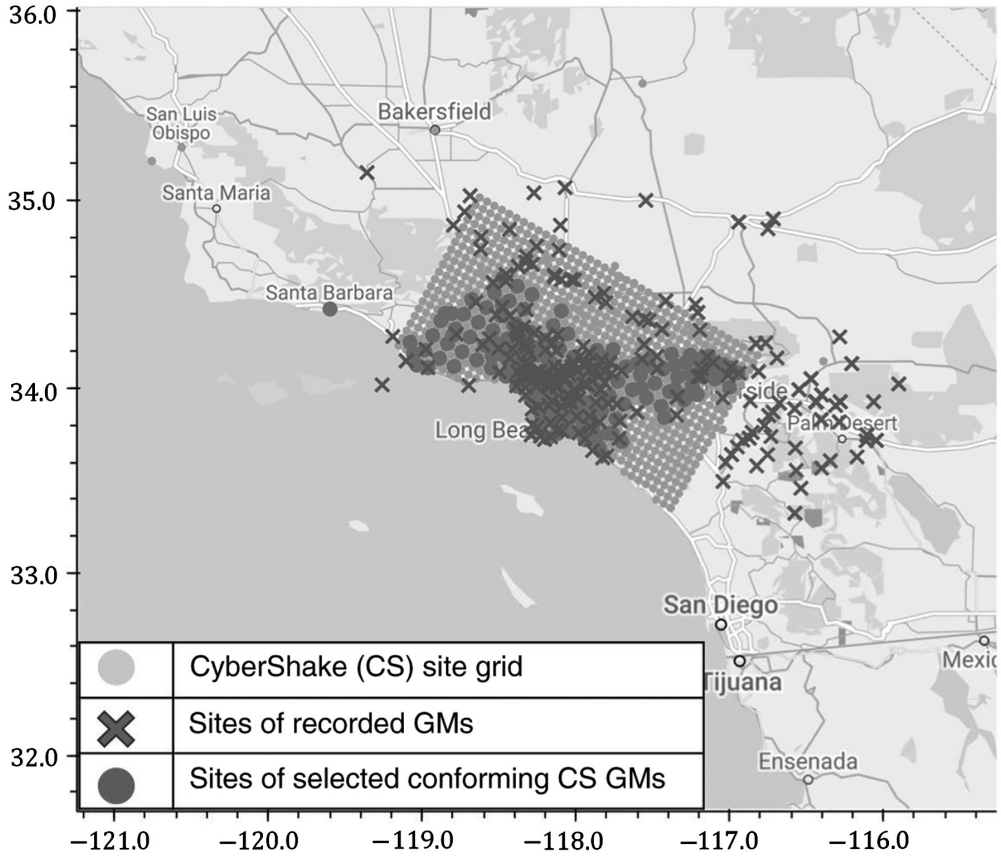

Figure 1. Sites of the selected recorded and simulated ground motions (GMs).

of coefficients from the simulated catalogs, to evaluate whether the same earthquake scenario (defined by $\boldsymbol{\theta}$) in the recorded and simulated catalogs leads to waveforms that result in similar EDP statistics.

Step 7: Using the event and site parameters and appropriate functional forms, develop and compare regression equations to estimate the $\mathbf{RZZ_s}$ ($\boldsymbol{\theta} \rightarrow \mathbf{RZZ_s}$) between the recorded set and the n catalogs of simulated ground motions

For both the recorded catalog and the n simulated catalogs, using appropriate functional forms, independent regressions are conducted between $\boldsymbol{\theta}$ and $\mathbf{RZZ_s}$. The fitted regression coefficients represent the effect of the physics of the rupture, wave propagation, and site effects on the $\mathbf{RZZ_s}$ obtained from the recorded and n simulated catalogs. The set of coefficients from the recorded catalog is statistically compared against the n sets of coefficients from the simulated catalogs, to evaluate whether the same scenario for simulated and recorded ground motions leads to statistically similar ground-motion parameters.

The described methodology allows the validation of a simulation method despite differences in the scenarios of recorded and simulated catalogs. It only requires the ranges, and where possible the distributions, of the event and site parameters (e.g., M_w, R_{rup}, V_{S30}), to be consistent in the recorded and simulated catalogs. To compare these catalogs and validate a simulation method, the effect of the event and site parameters on the EDP or $\mathbf{RZZ_s}$ is evaluated by developing regression models that account for the physics of earthquakes, wave propagation, and structural response to the extent possible, and then comparing the regression coefficients. The idea behind the proposed methodology is, hence, to compare the statistics of the $\mathbf{RZZ_s}$ and EDP, after correcting for the differences in the $\boldsymbol{\theta}$. A ground-motion simulation method is validated for an engineering application, if one can demonstrate three conditions: (1) the $\mathbf{RZZ_s} \rightarrow$ EDP process obtained from recordings belongs to the population of $\mathbf{RZZ_s} \rightarrow$ EDP processes from the simulated ground motions, (2) the $\boldsymbol{\theta} \rightarrow$ EDP process obtained from recordings belongs to the population of $\boldsymbol{\theta} \rightarrow$ EDP processes from the simulated ground motions, and (3) the $\boldsymbol{\theta} \rightarrow \mathbf{RZZ_s}$ process obtained from recordings belongs to the population of $\boldsymbol{\theta} \rightarrow \mathbf{RZZ_s}$ processes from the simulated ground motions. The combination of the first two conditions shows that the $\mathbf{RZZ_s}$ vector is capable of parameterizing the physics of ground motions (i.e., the simulated ground motions are validated) for the target application. Provided that the $\mathbf{RZZ_s}$ vector is efficient and sufficient in predicting EDP for both recorded and simulated motions, then the third condition can be used to validate current and future simulations of the target ground-motion simulation method for the considered engineering application.

DETAILED IMPLEMENTATION AND DISCUSSION

Step 1: For the region of interest, obtain the set of recorded ground motions and develop $n(> 50)$ catalogs of statistically conforming simulated ground motions.

Selection of recorded ground motions

The validation methodology proposed in this study is applied to the CyberShake source-based ground-motion simulations (Graves *et al.*, 2011), which are limited to events with $M_w \geq 6$ and to sites located in and around the Los Angeles basin in the southern California region, as illustrated by the light gray circles

TABLE 1
Recorded Seismic Events Used in This Study (from Next Generation Attenuation-West2 Database)

Earthquake Name	Date (yyyy/mm/dd)	Magnitude	Number of Recording Stations
Kern County	1952/07/21	7.36	2
San Fernando	1971/02/09	6.61	26
North Palm Springs	1986/07/08	6.06	33
Big Bear-01	1992/06/28	6.46	32
Hector Mine	1999/10/16	7.13	25
Landers	1992/06/28	7.28	24
Joshua Tree, California	1992/04/23	6.1	5
Northridge-01	1994/01/17	6.69	141

in Figure 1. For consistency, the dataset of recorded ground motions is developed by selecting from the Next Generation Attenuation-West2 (NGA-West2) database (Ancheta *et al.*, 2014) earthquakes with $M_w \geq 6$ and excluding aftershocks. The dataset is also limited to recording stations with $R_{rup} \leq 100$ km, 200 m/s $\leq V_{S30} \leq$ 750 m/s, and located within 100 km of a CyberShake site having 200 m/s $\leq V_{S30} \leq$ 750 m/s. This results in 288 recordings from eight earthquake events with $6 \leq M_w \leq 7.5$ and represents a seismicity of $TS = 100$ yr in the region. The sites of the recorded ground motions are shown by crosses in Figure 1, and the list of earthquakes is provided in Table 1.

Selection of simulated ground motions

Simulation of earthquake catalogs. The CyberShake database consists of broadband seismograms developed by combining low-frequency deterministic components with high-frequency stochastic components. As part of the CyberShake study, ground motions were simulated at 336 sites in southern California, for all the ruptures that are located within 200 km from each site. The ruptures considered are based on the second Uniform California Earthquake Rupture Forecast (UCERF2; Field *et al.*, 2009), with modifications that include constraining the ruptures to magnitudes larger than 6 and excluding background seismicity. The deterministic component of the seismograms is generated by solving the wave propagation equation within a 3D seismic-velocity structure, in which the minimum shear-wave velocity is set to 500 m/s (Graves *et al.*, 2011), and naturally accounts for basin and directivity effects, whereas the high-frequency component is computed using the method of Graves and Pitarka (2010) for hard-rock sites. To account for the nonlinear response of soft soils in the near surface, empirically based amplification factors are applied to both components before combining them at a frequency of 1 Hz. The V_{S30} of each site is determined from the Community Velocity Model (CVM-S4.26) developed by the Southern California Earthquake Center (SCEC). Each simulated ground motion in the CyberShake database corresponds to a scenario defined by an earthquake event and a site that is affected by this event.

Earthquake catalogs corresponding to a time span of $TS = 100$ yr are developed using the Monte Carlo simulation technique proposed by Azar *et al.* (2019) and the same source model as CyberShake. The 100 yr time span is selected for consistency with the time span of recorded seismicity and the number of recorded events in the southern California region. Each simulated catalog is considered as one realization of the possible earthquake events that could occur within 100 km of the CyberShake sites over a period of 100 yr. Alternative catalog simulation methods and earthquake rupture forecast models can be used to develop realistic simulated earthquake catalogs, for example, in other regions of interest.

Selection of the ground motions for each simulated catalog. After simulating an earthquake catalog, CyberShake sites are sampled for each event. The site selection process should ensure that the distribution of the site-specific parameters (mainly R_{rup} and V_{S30}) in the catalog of simulated ground motions is consistent with the corresponding distribution in the set of recorded ground motions. The following site sampling technique is applied to each earthquake event in a simulated catalog:

- Determine the CyberShake sites that are located within 100 km of the earthquake rupture ($R_{rup} \leq 100$ km) and have 200 m/s $\leq V_{S30} \leq$ 750 m/s. Denote the number of sites that satisfy the criteria for this event as $n_{available}$.
- Randomly sample $n_{selected}$ values of R_{rup} from the cumulative distribution function of R_{rup} in the catalog of recorded ground motions in which $n_{selected} = \min(n_{available}, 30)$. The maximum number of sites per event is set to 30, because it is representative of the average number of recordings per event in the recorded catalog. To each sampled value, assign the CyberShake site with the closest R_{rup} value.

After defining the earthquake events and the sampled sites for each event, the corresponding seismograms are extracted from the CyberShake database. The distribution of R_{rup} in the simulated catalog should be comparable to its distribution in the recorded set. For this purpose, the KL divergence (Kullback and Leibler, 1951) is determined as a measure of the difference between the two distributions of R_{rup}. A lower value of the KL divergence indicates less difference between the distributions of R_{rup} in the two catalogs.

With the relatively small sample size available (constrained geographically by the CyberShake simulations and in duration by the recordings), the fitted regression models are likely to vary, if other sample data from the same process is used (Burnham and Anderson, 2002). Although this effect cannot be gauged on the recorded set, it can be evaluated on the simulated catalog due to the availability of a large number of simulated ground motions. Hence, to account for this variability, simulated ground motions are sampled for $TS = 100$ yr time span, for $n = 100$ earthquake catalogs.

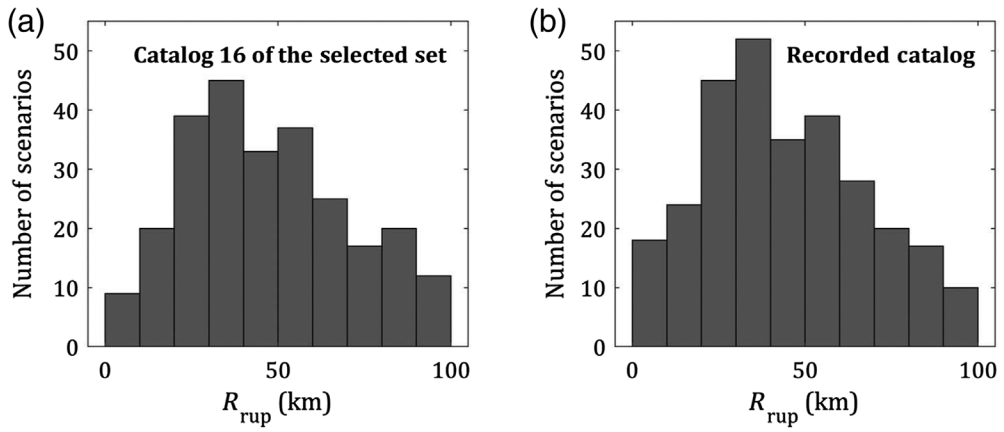

Figure 2. Histograms of R_{rup} of the scenarios (a) in catalog 16 of the selected set, and (b) in the catalog of recorded ground motions.

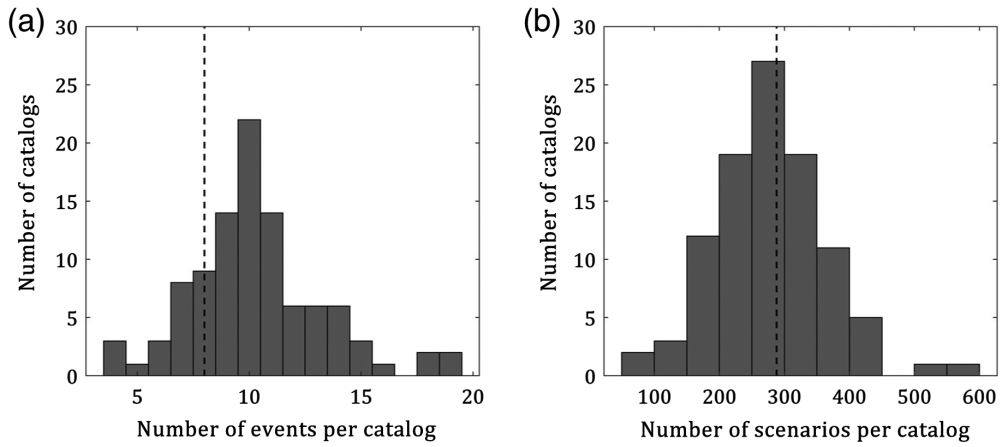

Figure 3. Distribution of (a) the number of events per catalog and (b) the number of scenarios per catalog in the selected set of catalogs. Dashed lines in (a,b) refer to the number of events and scenarios in the recorded catalog, respectively.

The range of M_w in the recorded dataset is between 6 and 7.5. In the simulated catalogs, the distribution of M_w is controlled by the source model used (a modified version of UCERF2), which includes events with M_w between 6 and 8.5. The catalog simulation process, by default, leads to some catalogs having a distribution of M_w similar to that of the recorded catalog, and to others that include events with M_w above 7.5 or lack events with M_w below 6.5. However, with a large number of CyberShake sites available, the distribution of R_{rup} in the simulated catalogs can be controlled, unlike that of M_w. To ensure that the distributions of R_{rup} are similar in the recorded and simulated datasets, 1000 sets of 100 simulated catalogs, each having a time span of 100 yr, are generated, based on the simulation technique and the site selection method described earlier. For each set, the distribution of R_{rup} in each simulated catalog is compared with the distribution of R_{rup} in the recorded catalog, by computing the KL divergence between the two distributions. This results in 1000 sets of 100 KL divergences that correspond to each set of 100 simulated catalogs. The set of 100 catalogs ultimately selected and used in this study is the one with the lowest KL mean (indicating that the distribution of R_{rup} in most of the 100 simulated catalogs is consistent with that of R_{rup} in the recorded catalog) and the lowest standard deviation (ensuring that the distributions of R_{rup} in the 100 simulated catalogs are similar to one another). Figure 2a and 2b shows the histograms of R_{rup} in one of the simulated catalogs of the selected set and in the recorded catalog, respectively. As expected, the distribution of R_{rup} in the simulated catalog is close to its distribution in the recorded catalog. The constraint on the regions of the recording and CyberShake sites to be geographically similar helps in naturally selecting recorded and simulated scenarios with similar site and path parameters.

Figure 3 presents the distribution of the number of events and scenarios per catalog for the selected set of 100 simulated catalogs. The average number of events per simulated catalog is 10, as compared to 8 in the recorded catalog, whereas the average number of scenarios per simulated catalog is 281, as compared to 288 in the recorded catalog. The CyberShake sites in the selected set of simulated catalogs are illustrated by the dark gray circles in Figure 1. The spectra of the recorded and finally selected simulated ground motions are shown in Figure 4. It is observed that, for shorter periods, the spectra of the simulated and recorded ground motions tend to be similar, whereas, for longer periods, simulated ground motions tend to be higher than recorded motions.

Step 2: Conduct NLTHA of the target structure to obtain the EDPs for the recorded catalog and n catalogs of simulated ground motions

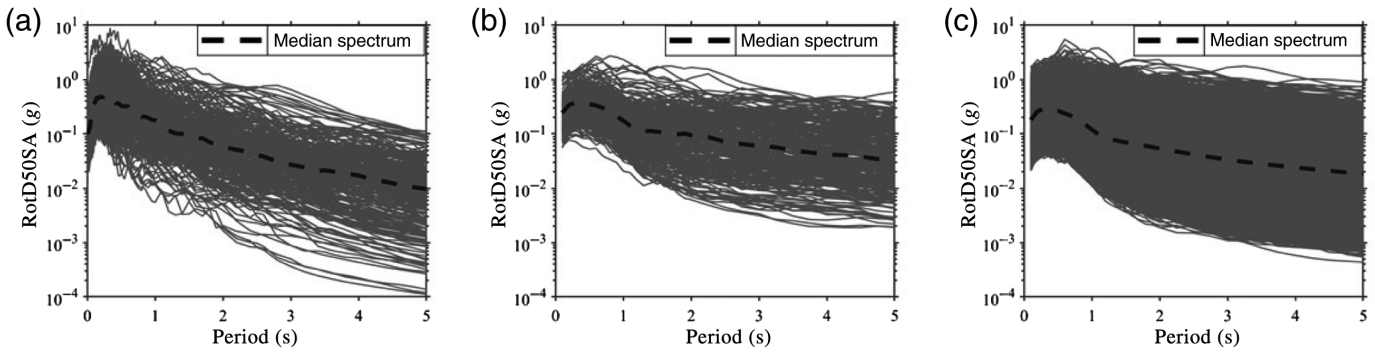

Figure 4. RotD50 spectra of (a) recorded ground motions, (b) catalog 97 of simulated ground motions, and (c) simulated ground motions from the combined 100 catalogs.

A single-column two-spanned box-girder bridge structure, described in Fayaz *et al.* (2020) as bridge A, is used as an example in this study for validation purposes. The bridge consists of two equal spans, each of 33.6 m length and 8.4 m width, a single column of radius 0.84 m and height 6.7 m consisting of 2% longitudinal reinforcement, and possesses a fundamental period of 0.61 s. The finite-element model of the bridge was developed in *OpenSees* (McKenna *et al.*, 2010). The model comprises seat-type abutments, a column bent, and an elastic superstructure that represents the deck. Because the behavior and performance of bridge structures are majorly deduced from the column drift ratio (CDR) of the central bent, maximum CDR is used as the EDP in this application. In particular, NLTHA is conducted by rotating the two orthogonal components of the ground motions from 0° to 180°, at intervals of 10° (18 intercept angles). For each intercept angle of the bidirectional ground-motion loading, its corresponding maximum CDR through the time history is obtained. The median of the 18 maximum CDRs is termed as Rot50CDR and used as the primary EDP in this research. Figure 5 shows the histograms of the Rot50CDR obtained from the NLTHA of bridge A, using recorded and 100 catalogs of simulated ground motions. The bridge A structure tends to yield around 0.9% CDR in the critical direction. Hence, it can be observed from Figure 5, the EDPs are primarily in the elastic range; however, some ground motions tend to push the bridge into nonlinearity.

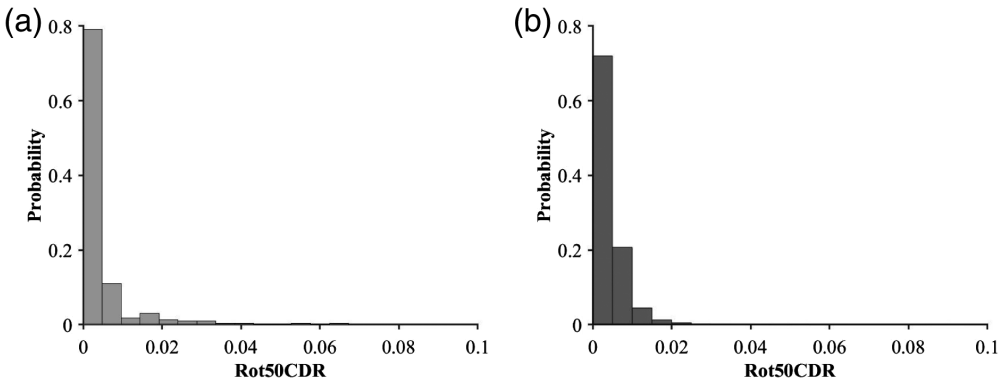

Figure 5. Histograms of Rot50CDR of bridge A under (a) recorded ground motions and (b) simulated ground motions (all catalogs combined).

Step 3: Compute the **RZZ** parameters of all the recorded and simulated ground motions, and select the important **RZZ** parameters that sufficiently describe the EDP of the target structure

As there are 16 parameters in the **RZZ** vector, it is essential to identify which of these are essential for performing the validation tests (i.e., to identify $\mathbf{RZZ_s}$). The prediction power of each **RZZ** parameter in describing Rot50CDR of the bridge structure, for both recorded and simulated motions, is of importance. This is done using the advanced wrapper algorithm of Boruta (Kursa and Rudnicki, 2010) coupled with the random forests algorithm (Zhu *et al.*, 2015). Because the Boruta algorithm is based on the random forests algorithm, it is a good choice to conduct the feature selection. Because of their nonparametric nature, random forests are robust and have a high power of handling datasets with high dimensionality and can deduce the highly nonlinear relationships among the features and target variables. Random forests also work very well with smaller datasets and handle the outliers better. The Boruta wrapper adds to the advantages of the random forests, by comparing the importance of features with their own randomized versions, to predict the target variable and then further eliminating the subjectivity of "important" features by comparing their importance against a binomial distribution. The most important features are ranked as 1, tentative features are ranked 2, and the noise-level features (features to be removed) are ranked greater than 2. This algorithm is performed for the recorded set and each simulated catalog independently. The results of Boruta for the **RZZ** parameters, to estimate Rot50CDR, are presented in Figure 6 for the recorded ground motions and for the

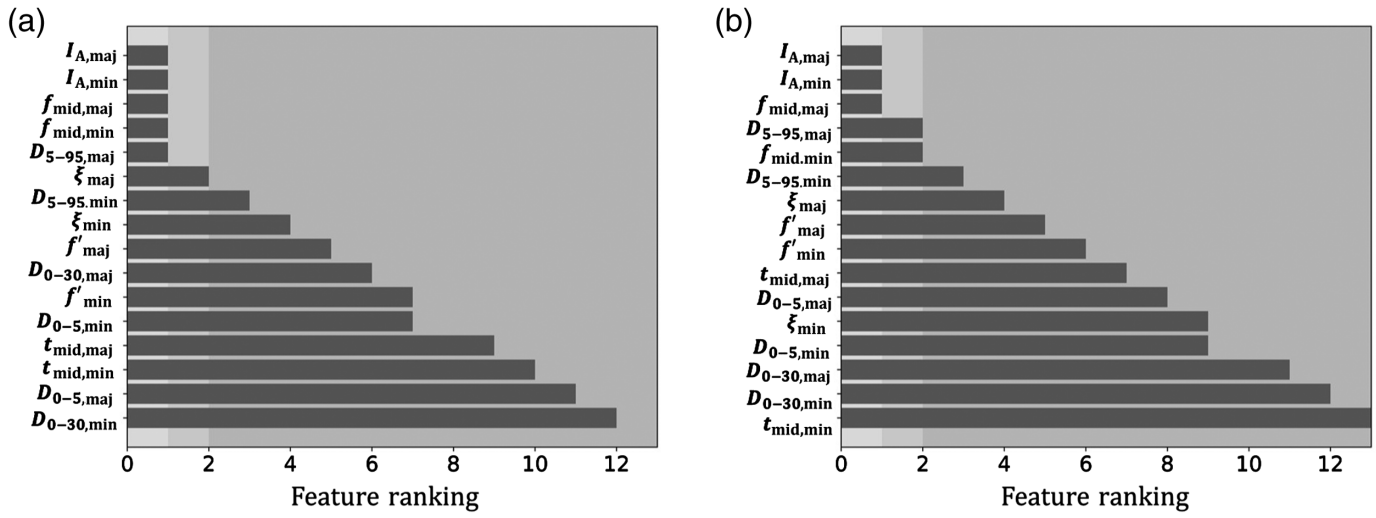

Figure 6. Feature ranking of **RZZ** parameters to estimate Rot50CDR using (a) recorded ground motions and (b) simulated ground motions from the combined 100 catalogs.

combination of all the simulated catalogs. The results for independently simulated catalogs are highly consistent with the result for all the catalogs combined. As can be seen from Figure 6, six parameters of **RZZ**, namely $I_{A,maj}$, $I_{A,min}$, $f_{mid,maj}$, $f_{mid,min}$, $D_{5-95,maj}$, and ξ_{maj} are classified as essential features (ranked 1 or 2) for the recorded and simulated ground motions; they are denoted as the important **RZZ** parameters.

Step 4: Among the important **RZZ** parameters drop the collinear parameters and obtain the finalized subset of $\mathbf{RZZ_s}$ parameters that can describe the EDP of the target structure

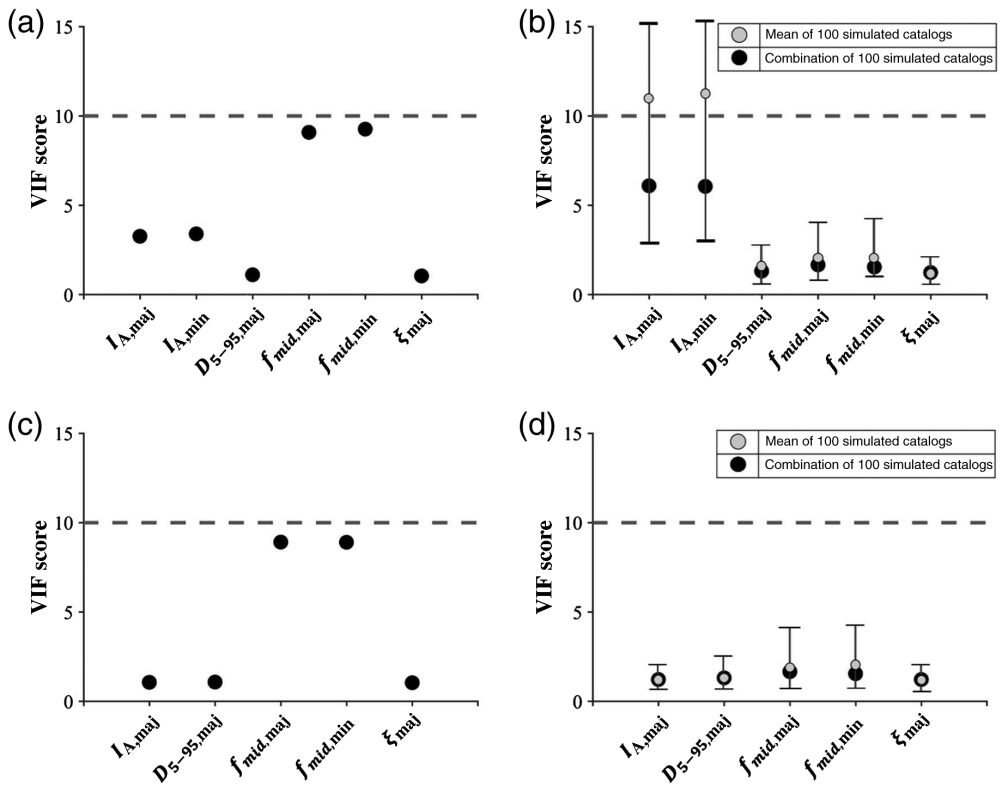

Figure 7. Variance inflation factor (VIF) of important **RZZ** parameters for (a) recorded ground motions, (b) simulated ground motions, (c) recorded ground motions after removing $I_{A,min}$, and (d) simulated ground motions after removing $I_{A,min}$.

Rezaeian and Der Kiureghian (2010) showed that the **RZZ** parameters are correlated, which can cause issues of multicollinearity in developing the regression equations. The VIF (James *et al.*, 2017) is used to detect multicollinearity. A VIF value above 10 suggests significant evidence for the presence of collinearity among the features. Figure 7a shows the VIFs for the important **RZZ** of the recorded ground motions, and Figure 7b presents the bands of the VIFs for the important **RZZ** of the 100 simulated catalogs, along with their mean values and the VIF computed by combining all the simulated catalogs together. It is noted that, although significant collinearity is not observed for recorded ground motions, for simulated motions some of the catalogs tend to show collinearity for $I_{A,maj}$ and $I_{A,min}$ (bands of

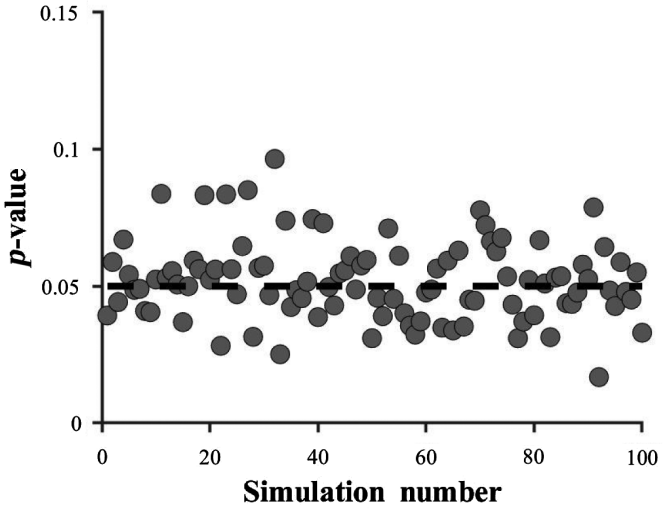

Figure 8. Results of the hypothesis test for similarity of $\mathbf{RZZ}_s$ correlation structure.

VIF lie above 10). Hence, $I_{A,min}$ is dropped, and the VIF test is repeated (see Fig. 7c,d). VIF < 10 indicates that the effect of collinearity is reduced. Hence, the five parameters $I_{A,maj}$, $D_{5-95,maj}$, $f_{mid,maj}$, $f_{mid,min}$, and ξ_{maj} are selected for the recorded and simulated ground motions to be denoted as $\mathbf{RZZ}_s$.

The Pearson correlation structures of the $\mathbf{RZZ}_s$ parameters in the recorded and simulated catalogs are compared, and their similarity is tested using the χ^2 test proposed by Satorra and Bentler (2010). The χ^2 test revealed that the hypothesis (that the correlation structure of the recorded catalog is not similar to that of a simulated catalog) is rejected at the 5% significance level (p-value = 0.05) for 52 out of the 100 catalogs. The results of the hypothesis test are presented in Figure 8. It is observed that the p-values tend to lie between 0.03 and 0.1. In general, the correlations of $I_{A,maj}$ with ξ_{maj} and of $f_{mid,maj}$ and $f_{mid,min}$ with $D_{5-95,maj}$ were observed to be higher (in absolute value) in simulated ground motions as compared with recorded motions. Other correlations are observed to be similar between recorded and simulated ground motions. It is concluded that, in general, the correlation structure of the $\mathbf{RZZ}_s$ for recorded motions can be considered similar to that of the simulated ground motions. However, it is suggested that the correlation structures within the $\mathbf{RZZ}_s$ are carefully evaluated for the CyberShake study.

Step 5: Using the $\mathbf{RZZ}_s$ parameters, develop and compare regression equations to estimate the EDP ($\mathbf{RZZ}_s \rightarrow$ EDP) between the recorded set and the n catalogs of simulated ground motions

Linear regression is conducted between the $\mathbf{RZZ}_s$ and EDP (i.e., Rot50CDR), using equation (1) for the recorded catalog and the 100 simulated catalogs. Because linear regression is widely used as the basic relation, to describe the effect of the features on the target variable, this study uses equation (1) as the link between $\mathbf{RZZ}_s$ and EDP (i.e., Rot50CDR). The VIF values were recalculated for the log-transformed $\mathbf{RZZ}_s$ parameters, to ensure that no issues of multicollinearity arise after the transformation, and they were

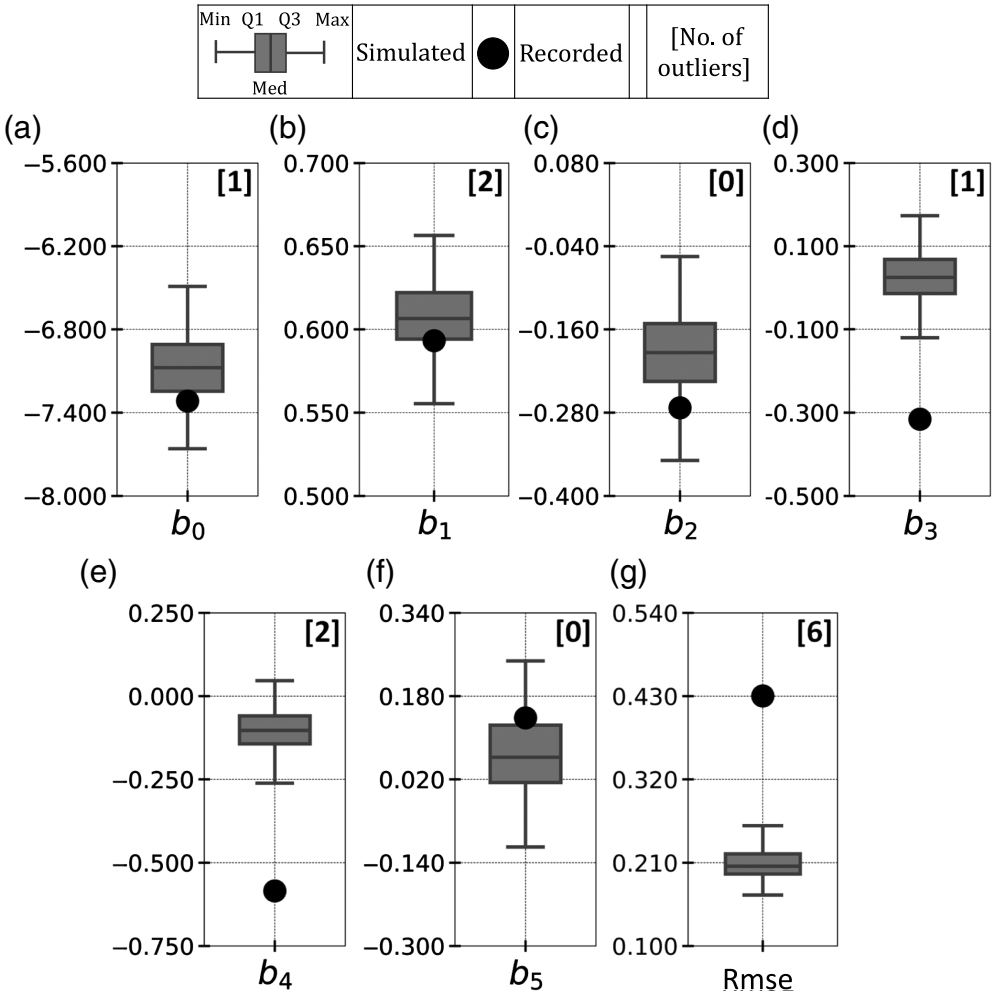

Figure 9. Comparison of simulated and recorded regression coefficients between $\mathbf{RZZ}_s$ and Rot50CDR: (a) b_0, (b) b_1, (c) b_2, (d) b_3, (e) b_4, (f) b_5, and (g) root mean square error (rmse).

all found to be below 10. The regression is conducted independently for the recorded catalog and for the 100 simulated catalogs. The result is one set of regression coefficients for the recorded catalog and 100 sets of coefficients for the simulated catalogs. For the recorded catalog, $R^2_{adj} = 0.76$ was observed for the fit, whereas for the simulated catalogs $R^2_{adj} = 0.83$ was observed on average (R^2_{adj} ranging from 0.77 to 0.86). Because in both cases, the regressions demonstrated high goodness of fit, it is postulated that the regression equations are capable of defining the trends, and thus that the selected $\mathbf{RZZ_s}$ parameters are efficient at predicting the EDP. Then, the 100 sets of coefficients obtained from simulated catalogs are compared against the set of coefficients obtained from the recorded catalog. To avoid making any assumptions on the distribution of the data, the comparison between the coefficients is made using box-and-whisker plots, as shown in Figure 9. Apart from the coefficients, the remaining noise is also compared in terms of their rmse. The box-and-whisker plot in the figures represents the values of the coefficients for the 100 simulated catalogs in which the ends of the boxes represent the 75th (third quantile, Q3) and 25th (first quantile, Q1) percentiles, the ends of whiskers represent the maximum and minimum values (excluding any outliers detected outside $Q1 - 1.5 \times (Q3 - Q1)$ or $Q3 + 1.5 \times (Q3 - Q1)$), and the line inside the box represents the median value (50th percentile). The dark circles in the figure represent the values of the coefficients obtained from the recorded set.

The coefficients of the regression model fitted to the recorded set tend to fall close to the interquartile range (Q1–Q3) for the coefficients associated with the intercept, $I_{A,maj}$, $D_{5-95,maj}$, and ξ_{maj}, but the coefficients associated with $f_{mid,maj}$ and $f_{mid,min}$ fall well below the minimum whiskers (see Fig. 9). Nonetheless, the work of Fayaz *et al.* (2020) proposed that among the **RZZ** parameters, $I_{A,maj}$ and $D_{5-95,maj}$ possess the highest prediction power, to capture the response of bridge structures, and the coefficients b_1 and b_2 associated with these parameters are similar in the recorded and simulated catalogs; thus, the recorded and simulated ground motions can be considered to be statistically similar in their mean $\mathbf{RZZ_s}$ to EDP relationship, despite the differences observed in the scaling with $\ln(f_{mid})$. Conversely, the variability of the $\mathbf{RZZ_s}$ to EDP relationship is different between recorded and simulated motions, as can be observed by the difference in rmse in Figure 9:

$$\overline{\ln(\text{Rot50CDR})} = b_0 + b_1 \ln(I_{A,maj}) + b_2 \ln(D_{5-95,maj}) + b_3 \ln(f_{mid,maj}) + b_4 \ln(f_{mid,min}) + b_5 \ln(\xi_{maj}). \quad (1)$$

Step 6: Using the event and site parameters and appropriate functional forms, develop and compare regression equations to estimate the EDPs ($\boldsymbol{\theta} \rightarrow$ EDP) between the recorded set and the n catalogs of simulated ground motions

The comparison of the regression relations $\boldsymbol{\theta} \rightarrow$ EDP helps in understanding whether the same rupture, path, and site characteristics lead to statistically similar structural responses, when simulated and recorded ground motions are used. Because the simulated ground motions are selected such that they are conforming to the recorded ground motions in terms of M_w, R_{rup}, and V_{S30}, the relations $\boldsymbol{\theta} \rightarrow$ EDP should be similar for completion of the validation procedure. To develop the regression between $\boldsymbol{\theta}$ and Rot50CDR, a modified version of the Campbell and Bozorgnia (2014; hereafter, CB14) form is utilized in this study. Therefore, and in addition to M_w, R_{rup}, and V_{S30}, the vector of event and site parameters $\boldsymbol{\theta}$ used in this application includes the parameters employed by the CB14 models such as the Joyner–Boore distance (R_{JB}), the closest distance to the surface projection of the top edge of the coseismic fault rupture plane measured perpendicular to its average strike (Ancheta *et al.*, 2014) (R_x), the width of the fault rupture plane (W), the rake angle ($\lambda°$), the depth to the top of the fault rupture plane (Z_{TOR}), the average dip angle of the fault rupture plane ($\delta°$), the median estimated value of PGA on rock with $V_{S30} = 1100$ m/s (A_{1100}), the depth to the 2.5 km/s shear-wave velocity horizon beneath the site ($Z_{2.5}$), and the hypocentral depth (Z_{hyp}). The original CB14 form represents the scaling of the natural logarithm of an intensity measure (e.g., pseudospectral accelerations or Arias intensity) with respect to the source terms (earthquake magnitude, style of faulting, hypocentral depth, fault dip), path terms (geometric and anelastic attenuation, hanging wall), and site terms (shallow site and basin responses). However, CB14 used a dataset of ground motions recorded worldwide and that covers a broad range of event and site parameters, including events with $3 \le M_w \le 7.9$ and R_{rup} values up to 500 km. On the other hand, this study is limited to events in southern California, with $M_w \ge 6$ and $R_{rup} < 100$ km, and does not include events from normal faulting. Therefore, the original functional form is altered in this study, to accommodate the limited dataset. The modifications include dropping the terms specific to the Japan region, the term related to normal faulting, as well as the fault dip and anelastic attenuation terms, because they only appear for $M_w < 5.5$ and $R_{rup} > 80$ km, respectively. Moreover, the quadrilinear functional form used by CB14, to model the scaling of the intensity measure with magnitude, and which includes breaks in scaling at $M_w = 4.5$, 5.5, and 6.5, is reduced to a single linear function for $M_w > 6$. The modified functional form of CB14 adopted in this study is given in equation (2). For ease of comparison, the regression coefficients (c_0–c_{18}) in equation (2) are labeled as in CB14. Based on the rake angle, the type of faulting indicator variable F_{RV}, is obtained; $F_{RV} = 1$ for reverse or reverse oblique faults ($30 < \lambda < 150$) and $F_{RV} = 0$ otherwise. The detailed definitions of the hanging-wall term f_{hng}, shallow site-response terms f_{site1} and f_{site2}, basin-response terms f_{sed1}

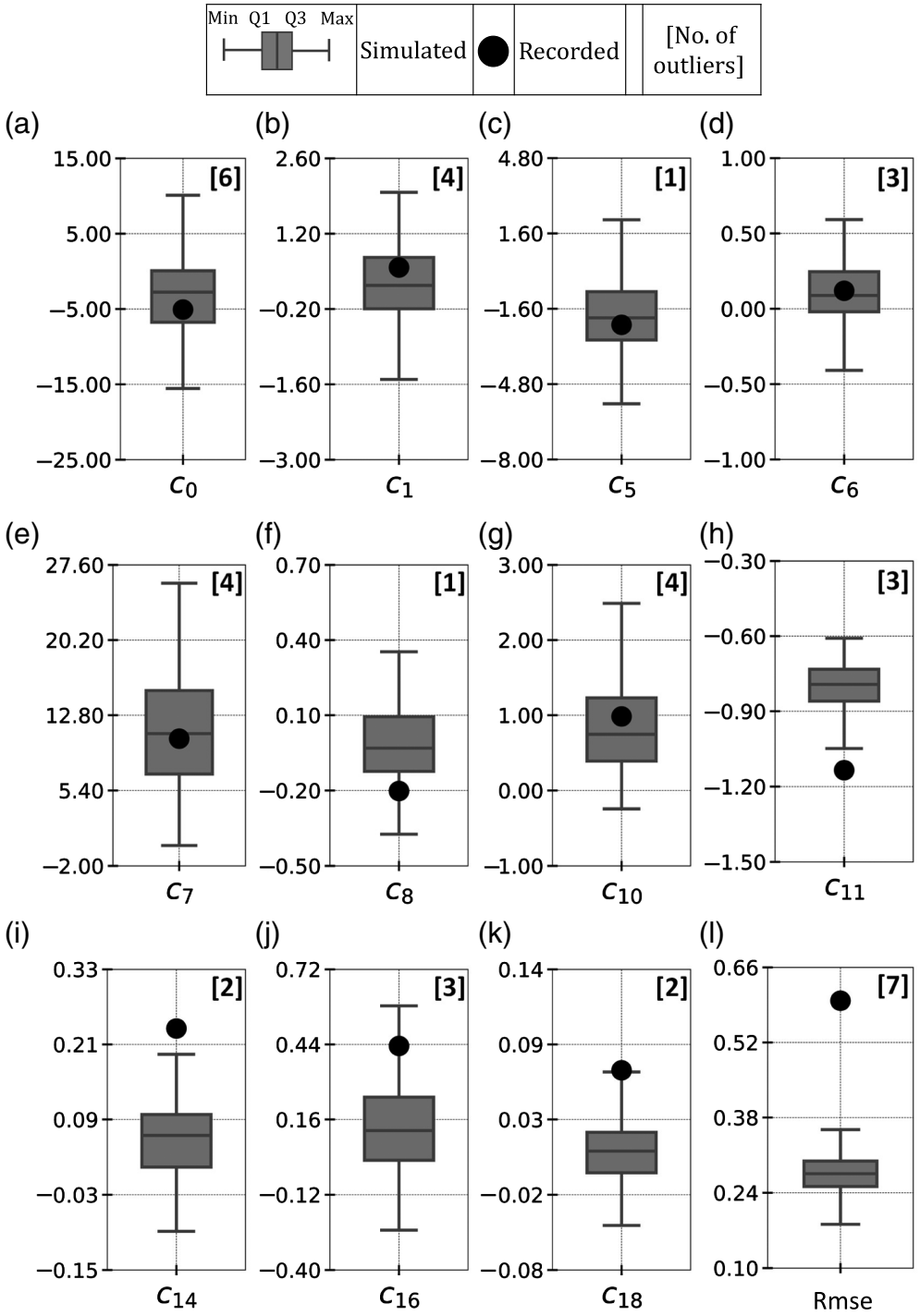

Figure 10. Comparison of simulated and recorded regression coefficients between **θ** and Rot50CDR: (a) c_0, (b) c_1, (c) c_5, (d) c_6, (e) c_7, (f) c_8, (g) c_{10}, (h) c_{11}, (i) c_{14}, (j) c_{16}, (k) c_{18}, and (l) rmse.

and f_{sed2}, and hypocentral depth term f_{hyp} can be found in the Appendix:

$$\overline{\ln(\text{Rot50CDR})} = c_0 + c_1 M_w + (c_5 + c_6 M_w)\sqrt{R_{\text{rup}}^2 + c_7^2} + c_8 F_{\text{RV}} + c_{10} f_{\text{hng}} + c_{11} f_{\text{site1}} + f_{\text{site2}} + c_{14} f_{\text{sed1}} + c_{16} f_{\text{sed2}} + c_{18} f_{\text{hyp}}. \quad (2)$$

The comparison of the coefficients of the regression is shown in Figure 10, where the box-and-whisker plots represent the values of the coefficients for the 100 simulated catalogs (excluding outliers), and the dark circles represent the coefficients of the recorded set. For the recorded set, $R_{\text{adj}}^2 = 0.73$ was observed for the fit, whereas for the simulated catalogs $R_{\text{adj}}^2 = 0.86$ was observed on average (with R_{adj}^2 ranging from 0.52 to 0.94). This demonstrates that the regression equations are capable of capturing the trends from event and site parameters to EDPs. As it is observed that the R_{adj}^2 values of **θ** → EDP are similar to those of $\mathbf{RZZ_s}$ → EDP, for both simulated and recorded catalogs; this proves the sufficiency of the $\mathbf{RZZ_s}$ parameters for the engineering application. Figure 10 shows that the fitted coefficients c_0, c_1, c_5, c_6, c_7, and c_{10} for the recorded set tend to fall within the interquartile ranges (Q1–Q3) of the simulated catalogs. This means that the effect of magnitude, geometric attenuation, and hanging wall on EDPs is similar between the recorded and simulated motions. Differences are mainly observed in coefficients c_{11} and c_{14}, which correspond to the site and basin effects. Further analysis is needed, such as studying more structures and exploring other regression functional forms, to better understand the cause of the observed differences. The seismic response of the studied bridge (with $T = 0.61$ s) is controlled by the stochastic high-frequency component of the CyberShake simulations. Therefore, different results could be observed for longer-period structures, with a seismic response dominated by the low-frequency component of the simulations. Lastly, similar to the $\mathbf{RZZ_s}$ to EDP relations, the R_{adj}^2 of the **θ** to EDP models fitted to the simulated catalogs

tend to be higher than the R^2_{adj} of the model fitted to the recorded motions. Moreover, the variability of the $\boldsymbol{\theta}$ to EDP relationship is different between recorded and simulated motions, as can be observed by the difference in rmse in Figure 10. This indicates that recorded ground motions tend to lead to higher variability in the responses than simulated ground motions for similar event parameters, as also noted by Star *et al.* (2011) and Galasso *et al.* (2012). However, in general, it is noticed that the mean relations between $\boldsymbol{\theta}$ and EDP are consistent between the simulated and recorded catalogs.

Step 7: Using the event and site parameters and appropriate functional forms, develop and compare regression equations, to estimate the $\mathbf{RZZ_s}$ ($\boldsymbol{\theta} \rightarrow \mathbf{RZZ_s}$) between the recorded set and the n catalogs of simulated ground motions

The functional forms to conduct the regressions for $\boldsymbol{\theta} \rightarrow \mathbf{RZZ_s}$ are selected from the available literature. For $I_{A,maj}$, the model proposed by Campbell and Bozorgnia (2019; hereafter, CB19), which is the same as the CB14 model, is used along with the modifications mentioned in the previous sections. The equation used for $I_{A,maj}$ is shown in equation (3) (similar to equation 2), and details of the model are given in the Appendix. However, for the regression model of $I_{A,maj}$, the coefficients of the magnitude–distance interaction term (c_6 and c_7) are fixed to the values fitted in CB19. Fitting c_6 and c_7 at the same time as c_1 and c_5 makes it difficult to compare the trends of $I_{A,maj}$ with magnitude and source-to-site distance (different combinations of the coefficients c_1, c_5, c_6, and c_7 among the various catalogs could lead to similar predictions of I_A). By constraining c_6 and c_7, the trends in the scaling of I_A as a function of magnitude and distance can be more accurately compared between the recorded and simulated catalogs. For the $\mathbf{RZZ_s}$ parameters $D_{5-95,maj}$, f_{mid} (the same model is used for $f_{mid,maj}$ and $f_{mid,min}$), and ξ_{maj}, the regression models are developed using the form of the predictive equations proposed in the site-based stochastic GMM of Dabaghi and Der Kiureghian (2018) and given by equations (4)–(6), respectively:

$$\overline{\ln(I_{A,maj})} = c_0 + c_1 M_w + (c_5 + c_6 M_w)\sqrt{R^2_{rup} + c_7^2} + c_8 F_{RV} + c_{10} f_{hng} + c_{11} f_{site1} + f_{site2} + c_{14} f_{sed1} + c_{16} f_{sed2} + c_{18} f_{hyp}, \quad (3)$$

$$\overline{\ln(D_{5-95,maj})} = \beta_0 + \beta_1 M_w + \beta_3 F_{RV} f_{flt,Z} + \beta_4 \ln\left(\sqrt{R^2_{rup} + 6^2}\right) + \beta_6 \ln V_{S30}, \quad (4)$$

$$\overline{\ln(f_{mid})} = \beta_0 + \beta_1 M_w + \beta_6 \ln V_{S30}, \quad (5)$$

$$\overline{\ln(\xi_{maj})} = \beta_0 + \beta_1 M_w + \beta_4 \ln\left(\sqrt{R^2_{rup} + 6^2}\right). \quad (6)$$

In equation (4), $f_{flt,Z} = Z_{TOR}$ if $Z_{TOR} < 1$ km and $f_{flt,Z} = 1$ if $Z_{TOR} \geq 1$ km. Figures 11–13 show the comparison of the regression coefficients between the recorded and simulated catalogs for the $\boldsymbol{\theta}$ to $\mathbf{RZZ_s}$ relations. Again, the box-and-whisker plots represent the values of the coefficients for the 100 simulated catalogs (excluding outliers), and the dark circles represent the coefficients of the recorded set. Figure 11 shows that the magnitude, style-of-faulting, hanging-wall, and hypocentral depth terms have similar effects on the $I_{A,maj}$ of both recorded and CyberShake ground motions, whereas the effect of the geometric attenuation term is less similar, as indicated by the coefficient c_5 for recorded motions lying outside the interquartile range of the simulated motions. There is a noticeable difference in the shallow site effects and basin effects. This is consistent with what is observed in the $\boldsymbol{\theta}$ to EDP relations. This further supports the hypothesis that the site and basin models used by CyberShake may need further analysis. In addition, the variability of $\ln I_{A,maj}$ in the recorded catalog is higher than the variability in most of the simulated catalogs, and the regression for recorded motions led to $R^2_{adj} = 0.94$, whereas the regressions of the simulated catalogs led to an average $R^2_{adj} = 0.98$ (and a range from 0.96 to 0.99). As a result, the rmse in the recordings-based regression model is higher than the rmse in all the simulation-based models. This indicates that the CyberShake simulations do not sufficiently reproduce the variability in the intensity of recorded ground motions, for given event and site parameters $\boldsymbol{\theta}$.

Figure 12 shows that the regression coefficients of $D_{5-95,maj}$ for the recorded catalog lie outside the interquartile ranges but within the minimum and maximum values of the coefficients for the simulated catalogs. This indicates that the CyberShake simulations well represent the scaling of duration with magnitude, source-to-site distance, style of faulting, and shallow site response. Moreover, the R^2_{adj} and rmse of the regression model for $D_{5-95,maj}$ fitted to recorded motions fall within the ranges of the R^2_{adj} and rmse of the regressions for simulated ground motions. For $f_{mid,maj}$, $f_{mid,min}$, and ξ_{maj}, the regression equations all lead to $R^2_{adj} < 0.5$. Therefore, the comparison between their remaining errors in terms of rmse is deemed more meaningful than the comparison of their coefficients (equations 5 and 6) and is illustrated in Figure 13. Comparison of the regression coefficients (not illustrated here) showed that the effect of M_w on $f_{mid,maj}$ and $f_{mid,min}$ is consistent in the simulated and recorded catalogs, but that the trends with V_{S30} are different. On the other hand, the rmse is observed to be consistent in the simulated and recorded catalogs for both $f_{mid,maj}$ and $f_{mid,min}$ (see Fig. 13a,b). For the damping parameter ξ_{maj}, the functional form of equation (6) yields a mean R^2_{adj} of 0.26 (ranging from 0.09 to 0.45) for the simulated catalogs, but an R^2_{adj} of only 0.04 for the recorded catalog. This indicates that the damping of simulated ground motions is better explained by the event and site parameters than the damping of the recorded motions. Differences are also observed in the ranges and distributions of ξ_{maj} in the two types of catalogs. These differences can be problematic, as they indicate that the damping parameter of the CyberShake simulated ground motions is

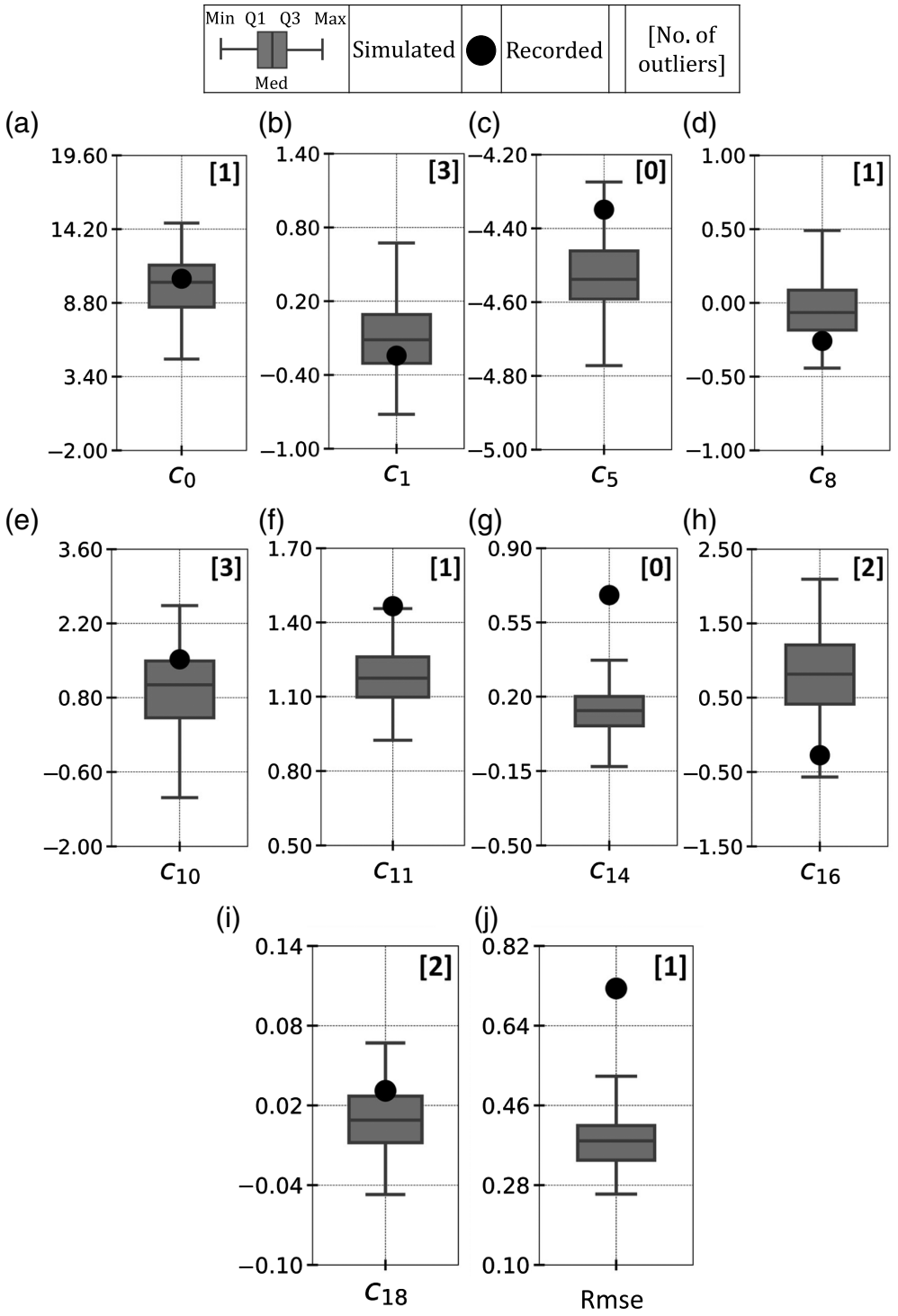

Figure 11. Comparison of simulated and recorded regression coefficients between $\boldsymbol{\theta}$ and $I_{A,maj}$: (a) c_0, (b) c_1, (c) c_5, (d) c_8, (e) c_{10}, (f) c_{11}, (g) c_{14}, (h) c_{16}, (i) c_{18}, and (j) rmse.

not statistically similar to that in recorded ground motions. This is also observed in the differences in rmse in Figure 13c.

CONCLUSIONS

A comprehensive methodology for validating simulated ground motion is presented; its application is demonstrated for CyberShake simulated motions and a bridge. The suggested validation methodology evaluates a ground-motion simulation method, by statistically comparing the similarity of three sets of relations obtained using simulated motions with the corresponding relations obtained using recorded motions. These three relations are between a vector of event and site parameters ($\boldsymbol{\theta}$), a vector of important ground-motion parameters ($\mathbf{RZZ_s}$), and an EDP of the engineering application.

Implementation of the suggested validation methodology for CyberShake and a bridge showed that the simulations could be used to assess the median seismic response of the bridge used for this validation exercise. During this exercise, it was observed that the scaling of $I_{A,maj}$, f_{mid}, and EDP of the simulated ground motions with the site- and basin-response terms is not statistically similar to that of the recorded motions. Further analysis of the trends in site and basin effects between recorded and simulated ground motions are required, to determine whether the observed differences are attributed to the simulation method or to the functional forms used in the regression models. Moreover, the variability of $I_{A,maj}$ and ξ_{maj} given $\boldsymbol{\theta}$, and of EDP given $\boldsymbol{\theta}$ or $\mathbf{RZZ_s}$ is larger in recorded motions compared with simulated motions. Aside from these differences, the three mean relations ($\boldsymbol{\theta} \rightarrow$ EDP, $\boldsymbol{\theta} \rightarrow \mathbf{RZZ_s}$, and $\mathbf{RZZ_s} \rightarrow$ EDP) tend to be statistically similar. The observations made about EDP are specific to the short-period bridge structure used in this article. Results may be different for structures with longer periods whose seismic response is controlled by the deterministic portion of the CyberShake simulations.

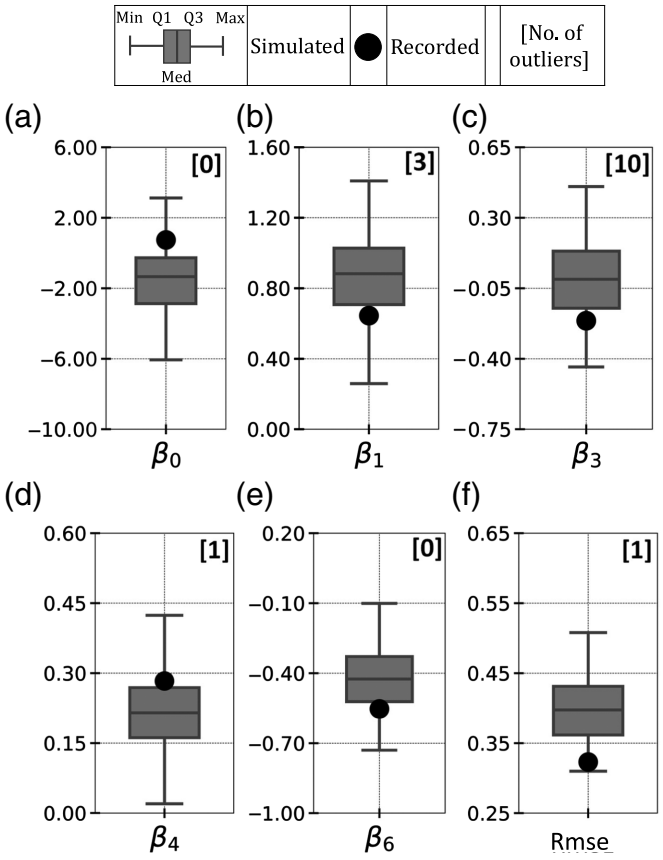

Figure 12. Comparison of simulated and recorded regression coefficients between $\boldsymbol{\theta}$ and $D_{5\text{–}95,\text{maj}}$: (a) β_0, (b) β_1, (c) β_3, (d) β_4, (e) β_6, and (f) rmse.

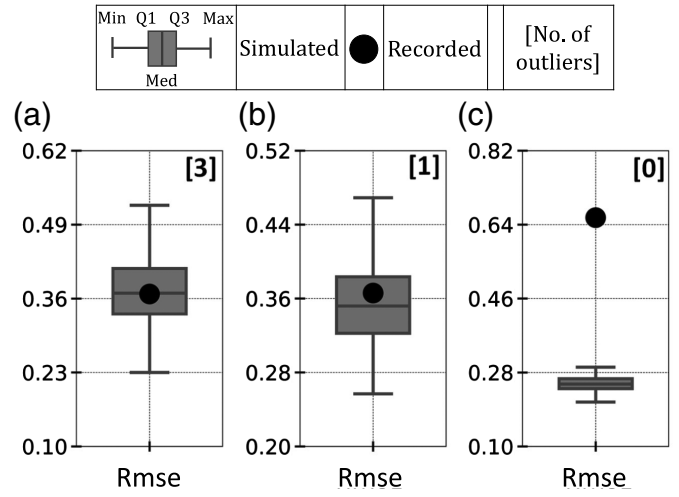

Figure 13. Comparison of rmse of simulated and recorded regression models between $\boldsymbol{\theta}$ and (a) $f_{\text{mid,maj}}$, (b) $f_{\text{mid,min}}$, and (c) ξ_{maj}.

The observations are also specific to the region of study and to the selected definition of EDP.

Because it is observed that the mean relations from $\mathbf{RZZ_s}$ to EDP are consistent and explanatory, it is proposed that $\mathbf{RZZ_s}$ be the first step of future validation exercises. Hence, based on the region of interest and application, it is proposed that recorded ground motions are obtained, and their **RZZ** vector are computed. Using the feature importance algorithm, $\mathbf{RZZ_s}$ is selected based on the intended application. Subsequently, the validation is conducted by comparing the simulated ground motions against the recorded ground motions, using the values of $\mathbf{RZZ_s}$, and the $\boldsymbol{\theta}$ to $\mathbf{RZZ_s}$ relations. Once the ground motions are validated for these, then the ground motions can be used to conduct structural analysis and further validated using the $\mathbf{RZZ_s}$ to EDP and $\boldsymbol{\theta}$ to EDP relations.

DATA AND RESOURCES

The data about CyberShake ground motions can be found at https://strike.scec.org/scecpedia/CyberShake_Study_15.12 (last accessed March 2020) and the CyberShake ground motions can be requested from Southern California Earthquake Center (SCEC; https://www.scec.org/, last accessed March 2020). The recorded ground motions can be obtained from Next Generation Attenuation-West2 (NGA-West2) database (https://ngawest2.berkeley.edu/, last accessed July 2018). The bridge structural model can be requested from https://faculty.sites.uci.edu/pbee/ (last accessed October 2020).

ACKNOWLEDGMENTS

This study is based on work supported by the Pacific Earthquake Engineering Research Center (PEER) Transportation Research Program under Grant Number 6640-001-0042. This financial support is gratefully acknowledged. Any opinions, findings, and conclusions or recommendations expressed in this article are those of the authors and do not necessarily reflect the views of sponsors. The authors thankfully acknowledge the valuable technical support from the Southern California Earthquake Center throughout this study.

REFERENCES

Ancheta, T. D., R. B. Darragh, J. P. Stewart, E. Seyhan, W. J. Silva, B. S.-J. Chiou, K. E. Wooddell, R. W. Graves, A. R. Kottke, and D. M. Boore (2014). NGA-West2 database, *Earthq. Spectra* **30,** 989–1005.

Azar, S., M. Dabaghi, and S. Rezaeian (2019). Probabilistic seismic hazard analysis using stochastic simulated ground motions, *13th International Conf. on Applications of Statistics and Probability in Civil Engineering*, Seoul, South Korea.

Bayless, J., and N. A. Abrahamson (2018). Evaluation of the interperiod correlation of ground-motion simulations, *Bull. Seismol. Soc. Am.* **108,** no. 6, 3413–3430.

Bijelić, N., T. Lin, and G. G. Deierlein (2019). Evaluation of building collapse risk and drift demands by nonlinear structural analyses using conventional hazard analysis versus direct simulation with CyberShake seismograms, *Bull. Seismol. Soc. Am.* **109,** no. 5, 1812–1828.

Bradley, B., D. Pettinga, J. F. Baker, and J. Fraser (2017). Guidance on the utilization of earthquake-induced ground motion simulations in engineering practice, *Earthq. Spectra* **33,** no. 3, 809–835.

Burnham, K. P., and D. R. Anderson (2002). *A Practical Information-Theoretic Approach, Model Selection and Multimodel Inference*, Second Ed., Springer, New York, New York.

Campbell, K. W., and Y. Bozorgnia (2014). NGA-West2 ground motion model for the average horizontal components of PGA, PGV, and 5% damped linear acceleration response spectra, *Earthq. Spectra* **30,** 1087–1115.

Campbell, K. W., and Y. Bozorgnia (2019). Ground motion models for the horizontal components of Arias intensity (AI) and cumulative absolute velocity (CAV) using the NGA-West2 database, *Earthq. Spectra* **35,** 1289–1310.

Dabaghi, M., and A. Der Kiureghian (2018). Simulation of orthogonal horizontal components of near-fault ground motion for specified earthquake source and site characteristics, *Earthq. Eng. Struct. Dynam.* **47,** 1369–1393.

Fayaz, J., M. Dabaghi, and F. Zareian (2020). Utilization of site-based simulated ground motions for hazard-targeted seismic demand estimation: Application for ordinary bridges in Southern California, *ASCE J. Bridge Eng.* **25,** no. 11, doi: 10.1061/(ASCE)BE.1943-5592.0001634.

Fayaz, J., M. Riquelme, and F. Zareian (2020). Sensitivity of the response of Box-Girder seat-type bridges to the duration of ground motions arising from crustal and subduction earthquakes, *Eng. Struct.* **219,** 110845.

Field, E. H., T. E. Dawson, K. R. Felzer, A. D. Frankel, V. Gupta, T. H. Jordan, T. Parsons, M. D. Petersen, R. S. Stein, R. J. Weldon II, *et al.* (2009). Uniform California Earthquake Rupture Forecast, version 2 (UCERF 2), *Bull. Seismol. Soc. Am.* **99,** 2053–2107.

Galasso, C., P. Kaviani, A. Tsioulou, and F. Zareian (2018). Validation of ground motion simulations for historical events using skewed bridges, *J. Earthq. Eng.* **24,** 1652–1674.

Galasso, C., F. Zareian, I. Iervolino, and R. W. Graves (2012). Validation of ground motion simulations for historical events using SDoF systems, *Bull. Seismol. Soc. Am.* **102,** no. 6, 2727–2740.

Galasso, C., P. Zhong, I. Zareian, and R. Graves (2013). Validation of ground motion simulations for historical events using MDoF systems, *Earthq. Eng. Struct. Dynam.* **42,** no. 9, 1395–1412.

Goulet, C. A., N. A. Abrahamson, P. G. Somerville, and K. E. Wooddell (2015). The SCEC broadband platform validation exercise: Methodology for code validation in the context of seismic-hazard analyses, *Seismol. Res. Lett.* **86,** no. 1, 17–26.

Graves, R., T. H. Jordan, S. Callaghan, E. Deelman, E. Field, G. Juve, C. Kesselman, P. Maechling, G. Mehta, K. Milner, *et al.* (2011). CyberShake: A physics-based seismic hazard model for Southern California, *Pure Appl. Geophys.* **168,** 367–381.

Graves, R. W., and A. Pitarka (2010). Broadband ground-motion simulation using a hybrid approach, *Bull. Seismol. Soc. Am.* **100,** 2095–2123.

James, G., D. Witten, T. Hastie, and R. Tibshirani (2017). *An Introduction to Statistical Learning*, Eighth Ed., Springer Science + Business Media, New York, New York, ISBN: 978-1-4614-7138-7.

Jones, P., and F. Zareian (2010). Relative safety of high-rise and low-rise steel moment-resisting frames in Los Angeles, *Struct. Des. Tall Spec. Build.* **19**, 183–196.

Kullback, S., and R. A. Leibler (1951). On information and sufficiency, *Ann. Math. Stat.* **22,** 79–86.

Kursa, M. B., and W. R. Rudnicki (2010). Feature selection with the Boruta package, *J. Stat. Software* **36,** no. 11, doi: 10.18637/jss.v036.i11.

McKenna, F., M. H. Scott, and G. L. Fenves (2010). Nonlinear finite element analysis software architecture using object composition, *J. Comput. Civ. Eng.* **24,** no. 1, 95–107.

Rezaeian, S., and A. Der Kiureghian (2010). Simulation of synthetic ground motions for specified earthquake and site characteristics, *Earthq. Eng. Struct. Dynam.* **39,** no. 10, 1155–1180.

Rezaeian, S., P. Zhong, S. Hartzell, and F. Zareian (2015). Validation of simulated earthquake ground motions based on evolution of intensity and frequency content, *Bull. Seismol. Soc. Am.* **105,** no. 6, 3036–3049.

Satorra, A., and P. M. Bentler (2010). Ensuring positiveness of the scaled difference chi-square test statistic, *Psychometrika* **75,** no. 2, 243–248.

Star, L., J. Stewart, and R. Graves (2011). Comparison of ground motions from hybrid simulations to NGA prediction equations, *Earthq. Spectra* **27,** 331–350, doi: 10.1193/1.3583644.

Tsioulou, A., A. A. Taflanidis, and C. Galasso (2019). Validation of stochastic ground motion model modification by comparison to seismic demand of recorded ground motions, *Bull. Earthq. Eng.* **17,** no. 6, 2871–2898.

Zhong, P. (2016). Ground motion simulation validation for building design and response assessment, *Ph.D. Dissertation*, University of California, Irvine, Irvine, California.

Zhu, R., D. Zeng, and M. R. Kosorok (2015). Reinforcement learning trees, *J. Am. Stat. Assoc.* **110,** no. 512, 1770–1784.

APPENDIX

Modified CB14 (CB19) functional form for Arias intensity and EDP

This Appendix provides details of the regression models developed in this article for the Arias intensity (I_A) and engineering demand parameter (EDP) (Rot50CDR) from recorded and simulated ground motions. The functional form used by Campbell and Bozorgnia (2014, 2019; hereafter, CB14 and CB19) is adapted to the limited dataset of this study. The modified functional form adopted is given in equation (A1), in which y represents $I_{A,maj}$, and Rot50CDR for the $\boldsymbol{\theta}$ to $I_{A,maj}$ and $\boldsymbol{\theta}$ to EDP mean predictive relations, respectively:

$$\ln(y) = c_0 + c_1 M_w + (c_5 + c_6 M_w)\sqrt{R_{rup}^2 + c_7^2} + c_8 F_{RV} + c_{10} f_{hng} + c_{11} f_{site1} + f_{site2} + c_{14} f_{sed1} + c_{16} f_{sed2} + c_{18} f_{hyp}. \quad \text{(A1)}$$

Hanging-wall term.

$$f_{hng} = f_{hng,R_x} f_{hng,R_{rup}} f_{hng,M} f_{hng,\delta}. \quad \text{(A2)}$$

The definitions of f_{hng,R_x}, $f_{hng,R_{rup}}$, and $f_{hng,\delta}$ are not reported, because no modifications to CB14 were applied.

However, after dropping the magnitude breaks, $f_{\text{hng},M}$ is defined as follows:

$$f_{\text{hng},M} = 1 + a_2(M_{\text{w}} - 6.5). \tag{A3}$$

The values of a_2 are taken from CB19 for $I_{\text{A,maj}}$, and from CB14 for spectral acceleration (SA)($T = 0.5$ s) (closest available period to the period of bridge A) for Rot50CDR.

Shallow site-response terms.

$$f_{\text{site}_1} = \ln V_{S30}/k_1, \tag{A4}$$

$$f_{\text{site}_2} = \begin{cases} k_2\{\ln\left[A_{1100} + c\left(\frac{V_{S30}}{k_1}\right)^n\right] - \ln[A_{1100} + c]\}; & V_{S30} \le k_1 \\ k_2 n \ln\left(\frac{V_{S30}}{k_1}\right). & V_{S30} > k_1 \end{cases}. \tag{A5}$$

The coefficients k_1, k_2, c, and n are assigned the values fitted by CB19 for $I_{\text{A,maj}}$, and by CB14 for SA($T = 0.5$ s) for Rot50CDR.

Basin-response terms.

$$f_{\text{sed}_1} = \begin{cases} Z_{2.5} - 1; & Z_{2.5} \le 1 \\ 0; & Z_{2.5} > 1 \end{cases}, \tag{A6}$$

$$f_{\text{sed}_2} = \begin{cases} 0; & Z_{2.5} \le 3 \\ k_3 e^{-0.75}[1 - \mathrm{e}^{-0.25(Z_{2.5}-3)}]; & Z_{2.5} > 3. \end{cases} \tag{A7}$$

Coefficient k_3 is assigned the value in CB19 for $I_{\text{A,maj}}$ and in CB14 for SA($T = 0.5$ s) for Rot50CDR.

Hypocentral depth term.

$$f_{\text{hyp}} = \begin{cases} 0; & Z_{\text{hyp}} \le 7 \\ Z_{\text{hyp}} - 7; & 7 < Z_{\text{hyp}} \le 20 \\ 13; & Z_{\text{hyp}} > 20 \end{cases}. \tag{A8}$$

Manuscript received 16 July 2020
Published online 8 December 2020